Bull. Mater. Sci., Vol. 37, No. 1, February 2014, pp. 27–33. © Indian Academy of Sciences.

Bath temperature impact on morphological evolution of $Ni(OH)_2$ thin films and their supercapacitive behaviour

U M PATIL[a,*], K V GURAV[b], J H KIM[b], C D LOKHANDE[c] and S C JUN[a]

[a]Department of Mechanical Engineering, Yonsei University, Seoul 120-749, Korea
[b]Thin Film Photonic and Electronics Lab, Department of Material Science and Engineering, Chonnam National University, 300 Yongbong-Dong, Puk-Gu, Gwangju 500-757, S. Korea
[c]Thin Film Physics Laboratory, Department of Physics, Shivaji University, Kolhapur 416 007, India

MS received 28 November 2012; revised 13 May 2013

Abstract. **Nanostructured $Ni(OH)_2$ thin films were deposited over stainless steel (SS) and glass substrate via simple chemical bath deposition (CBD) method. $NiCl_2$:$6H_2O$ were used as source of nickel and aqueous ammonia as a complexing agent. The coating process of $Ni(OH)_2$ material over substrate is based on the decomposition of ammonia complexed nickel ions at two different bath temperatures. The changes in structural, morphological and electrochemical properties are examined as an impact of bath temperature. XRD studies reveal formation of mixed phase of α and β at lower bath temperature (313 K) while, pure β phase of $Ni(OH)_2$ thin films deposited was observed at higher bath temperature (353 K). The morphological evolution from honeycomb structure to vertically aligned flakes over the substrate is observed as the influence of bath temperature. The supercapacitive performance based on the morphology examined by using cyclic voltammetric measurements in 1 M KOH. The maximum specific capacitances of 610 and 460 F/g were observed for the vertical flake and honeycomb structured $Ni(OH)_2$ thin films, respectively.**

Keywords. **$Ni(OH)_2$; chemical bath deposition; structural analysis; surface morphology; supercapacitive behaviour.**

1. Introduction

Electrochemical capacitors (supercapacitor) are being payed attention as an energy storage device due to its high power density, high charge/discharge cycle life and high energy efficiency (Largeot *et al* 2008; Wang *et al* 2012). So due to such extensive electrochemical properties, supercapacitor can be used in such a device, which requires high energy in a very short time. On the basis of storage mechanism, there are two types of supercapacitor, electrical double-layer (EDLC) and redox (pseudo capacitance) supercapacitors (Kandalkar *et al* 2010). The charge storage in double-layer supercapacitors is achieved by the formation of a double layer on the surface of the electrode material, whereas in redox supercapacitors, charge is stored on both the electrode surfaces through bulk of the material via Faradaic reaction. Therefore, charge stored in redox supercapacitors is greater than double-layer counterparts (Kandalkar *et al* 2010).

Subsequently, the pseudocapacitance comes mainly from the reversible redox reactions of the electro-active materials and conducting polymers and transition metal oxides/hydroxides are considered as promising material for redox supercapacitors (Cai *et al* 2004). Large surface area is an essential criterion to achieve larger capacitance. So many researchers find it interesting to develop different nanostructures of redox material in such a manner as it can offer large surface area and large pore volume for easy access to redox electrolyte (Matsui *et al* 2002; Yang *et al* 2004).

Nanostructured nickel hydroxide [$Ni(OH)_2$], one of the most important transition metal hydroxides, has received increasing attention due to its extensive applications, especially as a positive electrode active material, in alkaline rechargeable Ni-based batteries. Besides, it is well known that the crystallographic state, morphology and chemical composition of $Ni(OH)_2$ material are key parameters, which determine the electrochemical behaviour. $Ni(OH)_2$ with different nanostructures has been fabricated, such as tubes (Coudun and Hochepied 2005) and rods (Wang *et al* 2005) by template synthesis, nanoribbon by hydrothermal method (Liang *et al* 2004), stacks of pancakes by a chemical method (Chen and Gao 2005), hollow spheres by a simple solution chemistry method and sheet-like geometry by the hydrothermal method (Liu *et al* 2005; Ni *et al* 2005; Wu *et al* 2006).

However, one-step simple fabrication of $Ni(OH)_2$ active material with high surface area remains a considerable challenge. To optimize functional properties of the nanostructures for electrochemical applications, self-assembly method has been crucial. However, full knowledge and precise control of the self-assemble process are still difficult. The surface engineering research and industrial applications need

*Author for correspondence (ump_umakant@yahoo.com)

low-cost processing methods for large-scale production of materials with necessary performance and engineered surface. One such method, which is simple, low cost and applicable for large-scale production is chemical bath deposition (CBD) which has its own advantages such as simplicity, reproducibility, non-hazardous, cost effectiveness, etc (Mane and Lokhande 2000; Pawar *et al* 2011). Thus, CBD method has been preferred over other expensive methods (Cao *et al* 2007). In order to improve physical and electrochemical performance of devices, manufacturing $Ni(OH)_2$ morphology is the focus of current research.

In the present work, we synthesized $Ni(OH)_2$ thin films at two different bath temperatures (313 and 353 K) from an alkaline nickel chloride solution by adopting ammonia as complexing agent for complexion with good controllability and reproducibility. Subsequently effect of bath temperature on physicochemical characteristics such as structural, morphological and electrochemical properties of material was systematically studied. In addition, we have proposed schematic model for the evolution of microstructure as an effect of bath temperature on growth and distribution of $Ni(OH)_2$ onto substrate in thin film form.

2. Experimental

The nanocrystalline $Ni(OH)_2$ thin films have been deposited by CBD method at different bath temperatures lower (313 K) and higher (353 K), on glass and stainless steel substrates. The source of Ni used was 0·1 M $Ni(Cl)_2{\cdot}6H_2O$ and to make it alkaline, aqueous ammonia was added. Primarily precipitate of $Ni(OH)_2$ occurs which gets dissolved after further addition of aqueous ammonia. The resultant pH of solution was ~12. The stainless steel cleaned by fine polish paper (0·5 grade) and glass microslides were washed with detergent, followed by rinsing with double-distilled water and finally treated with ultrasonic waves for 15 min. These cleaned substrates were immersed in the prepared bath. When the bath attained the desired temperature, precipitation was started in the bath. During precipitation, heterogeneous reaction occurred over substrate surface and growth of $Ni(OH)_2$ took place. The substrates coated with $Ni(OH)_2$ thin films were taken out from the bath, dried in air and preserved in an airtight plastic container before examining the properties.

The thickness of nickel hydroxide film was measured by the weight difference method using a sensitive microbalance. Structural identification of nickel hydroxide films was carried out with X-ray diffractometer (XRD) (copper target ($\lambda = 1{\cdot}54056$ Å)). The microstructures of films were examined with a scanning electron microscope (SEM) (JEOL–JAPAN 6360). Electrochemical analysis of the films deposited on steel substrates was studied by cyclic voltammetry (CV) using a potentiostat (263A EG&G, Princeton Applied Research Potentiostat). The electrochemical cell comprises of a platinum counter electrode, saturated calomel, a reference electrode (SCE) and $Ni(OH)_2$, working electrode immersed in 1 M KOH electrolyte. All potentials are recorded and reported with respect to SCE.

3. Results and discussion

3.1 *Film formation mechanism*

Thin film formation in CBD method was observed when the solution attains supersaturated state (Hodes 2002). At supersaturated condition ionic product exceeds solubility product of the metal hydroxide, precipitation occurs and ions combine on the substrate to form nuclei. Further film growth can take place by ion-by-ion condensation of materials or by adsorption of colloidal particles from the solution on the substrate (Lokhande *et al* 2005; Shinde *et al* 2007). Nickel hydroxide thin films have been deposited on steel substrates by slow hydrolysis of nickel chloride solution. This can be represented by as follows.

First, nickel chloride ($NiCl_2{\cdot}6H_2O$) was complexed with ammonia (NH_3), a white precipitate of $Ni(OH)_2$ appears first, according to the reaction:

$$Ni^{2+} + 2OH^- \rightarrow Ni(OH)_2 \downarrow . \quad (1)$$

Further addition of NH_3 solution, $Ni(OH)_2$ precipitate redissolved into the solution, reaction leading into the formation of soluble $Ni(NH)_3^{4+}$ complex

$$Ni(OH)_2 + 4NH_3 \rightarrow Ni(NH)_3^{4+} + 2OH^- . \quad (2)$$

As bath temperature and deposition time prolongs, Ni^{2+} ions slowly dissociates from $Ni(NH)_3^{4+}$ complex and reacts with OH^- ions, to form $Ni(OH)_2$:

$$Ni(NH)_3^{4+} + 2OH^- \rightarrow Ni(OH)_2 + 4NH_3 \uparrow . \quad (3)$$

Bath temperature directly determines the decomposition rate of ammonia metal ion complex and changes nucleation rate and growth rates of nanocrystals. On the basis of bath temperature effect, growth rate of materials in thin film form with respect to deposition time is shown in figure 1. The film thickness is measured in terms of weight deposited on

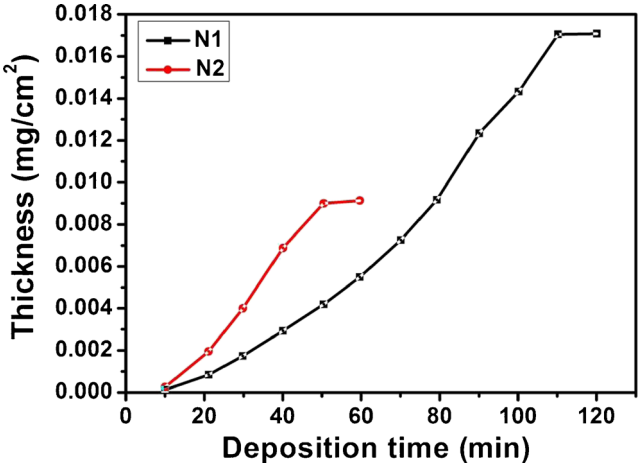

Figure 1. Plot of thickness as a function of deposition time for $Ni(OH)_2$ thin films prepared at (N1) 313 and (N2) 353 K temperatures.

unit area of substrate (Patake and Lokhande 2008). The film thickness of nickel hydroxide increases with deposition time, reaches a maximum value [N1 (313 K) = 0·017 and N2 (353 K) = 0·009 mg·cm^{-2}] and then almost remains constant. Hereafter, samples are referred to as N1 and N2 for sample prepared at lower and higher temperature, respectively. Deposition time for both samples are different; it affects due to different bath temperatures consequently by different growth rates. At lower bath temperature (N1), the decomposition rate of ammonia complex is a little slower, which resulted in a slower growth rate of material formation. However, higher bath temperature (N2) leads to quicker decomposition rate of ammonia complex and produces faster growth of material on the substrate. Sample N1 shows higher thickness as compared to sample N2, due to the faster growth rate resulting into quick formation of precipitation and settle down at container instead of growing over substrate (Salunkhe *et al* 2009).

3.2 *Structural analysis*

X-ray diffraction study was carried out for the determination of crystal structure along with structural changes and identification of phases of prepared $Ni(OH)_2$ thin films. Figure 2 shows XRD patterns of polycrystalline $Ni(OH)_2$, for samples N1 deposited at 313 and N2 deposited at 353 K, respectively. XRD pattern of sample N1 shows formation of mixed α and β phases of $Ni(OH)_2$ at lower temperature (313 K) while pure β phase was observed at higher temperature (353 K) (JCPDS card nos. 01-1047 and 74-2075 Yang *et al* 2007). Two factors are important in transformation of phase α–β of $Ni(OH)_2$, viz., the expulsion of intercalative water and ions (i.e. Cl^-) in α phase and adjustment of the stacking orders of $Ni(OH)_2$ layers. In earlier reports, the phase transformation α–β $Ni(OH)_2$ can be easily performed in the presence of alkali through chemical aging (Bernard *et al* 1996). The high reaction temperature favours transformation process above and provides driving force and energy to restructure the stacking order of $Ni(OH)_2$ layers. Thus, low temperature allows the formation of mixed (α and β) phases of $Ni(OH)_2$ and high temperature favours the formation of β $Ni(OH)_2$ (Tong *et al* 2012).

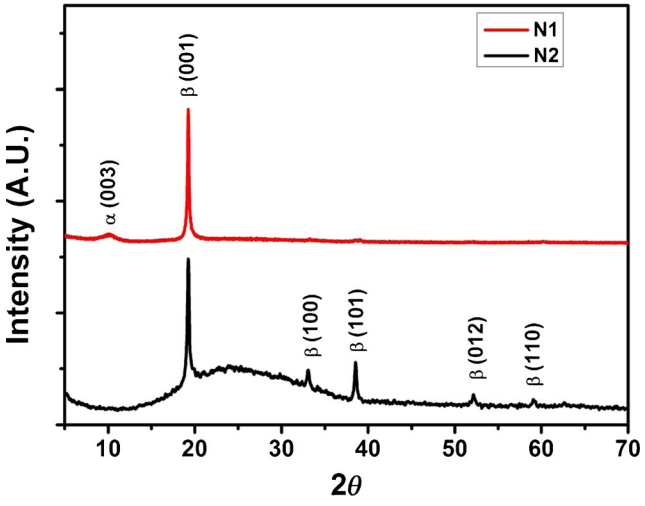

Figure 2. XRD patterns of $Ni(OH)_2$ thin films prepared at (N1) 313 and (N2) 353 K temperatures.

3.3 *Surface morphology*

The morphological change as an impact of bath temperature was studied by using SEM images. SEM micrographs of a '$Ni(OH)_2$' thin film prepared at different bath temperatures are presented in figure 3(a). The morphology of $Ni(OH)_2$ prepared at low bath temperature (313 K) is shown in figures 3(a, b). The film is porous and well covered with overgrown particles on the substrate. The surface morphology at higher magnification (figure 3(b)) is seen to be a well-covered, interconnected, macroporous, honeycomb-like structure. However, figures 3(c and d) shows SEM image of $Ni(OH)_2$ thin film prepared at high bath temperature (353 K). Figure 3(c) shows formation of microflowers comprising of vertical nanoflakes. SEM image at higher magnification shown in figure 3(d) reveals that flakes are vertically grown on substrate surface. The morphology reveals a mesoporous structure. The flake and honeycomb-like morphologies lead to a high specific surface area and porous volume, which provide the structural foundation for the high specific capacitance (Patil *et al* 2009; Gurav *et al* 2010).

Schematic growth model for bath temperature influenced by $Ni(OH)_2$ thin films is shown in figure 3(b) which supports growth kinetics for morphology alteration. Chemical bath deposition is one of the well known 'bottom-up' approaches based on the formation of a solid phase upon transformation of a supersaturated solution to the saturated state. This transformation incorporated with various distinct steps such as nucleation, coalescence and subsequent growth by aggregation of the particles. During nucleation, clusters of metal precursor molecules are likely to undergo rapid decomposition. Such nucleation centres acted as foundation for aggregation of the particles. Moreover, basic groundwork for the nanostructure is formed by coalescence of aggregated particles. Reaction bath temperature is a strategic factor that affects on structural and chemical properties of the $Ni(OH)_2$ product. The growth kinetic is slow at lower temperature, 313 K, so one-dimensional (1 D) growth of nanospecies takes place which leads to the formation of honeycomb morphology. However, rise in bath temperature results in the increase in reaction rate, so $Ni(OH)_2$ grains grown rapidly, which leads to the formation of flake-like morphology (2 D) comprising bunch of microflakes. Such change in growth kinetics at higher bath temperature is due to breaking rate of complexed metal ions which release more metal ions for rapid nucleation and the growth process resulted in the formation of 2 D flakes. The morphology evolution of $Ni(OH)_2$ as influence of bath temperature is due to nanodomains getting squeezed together into bunch of microflakes to form flower-

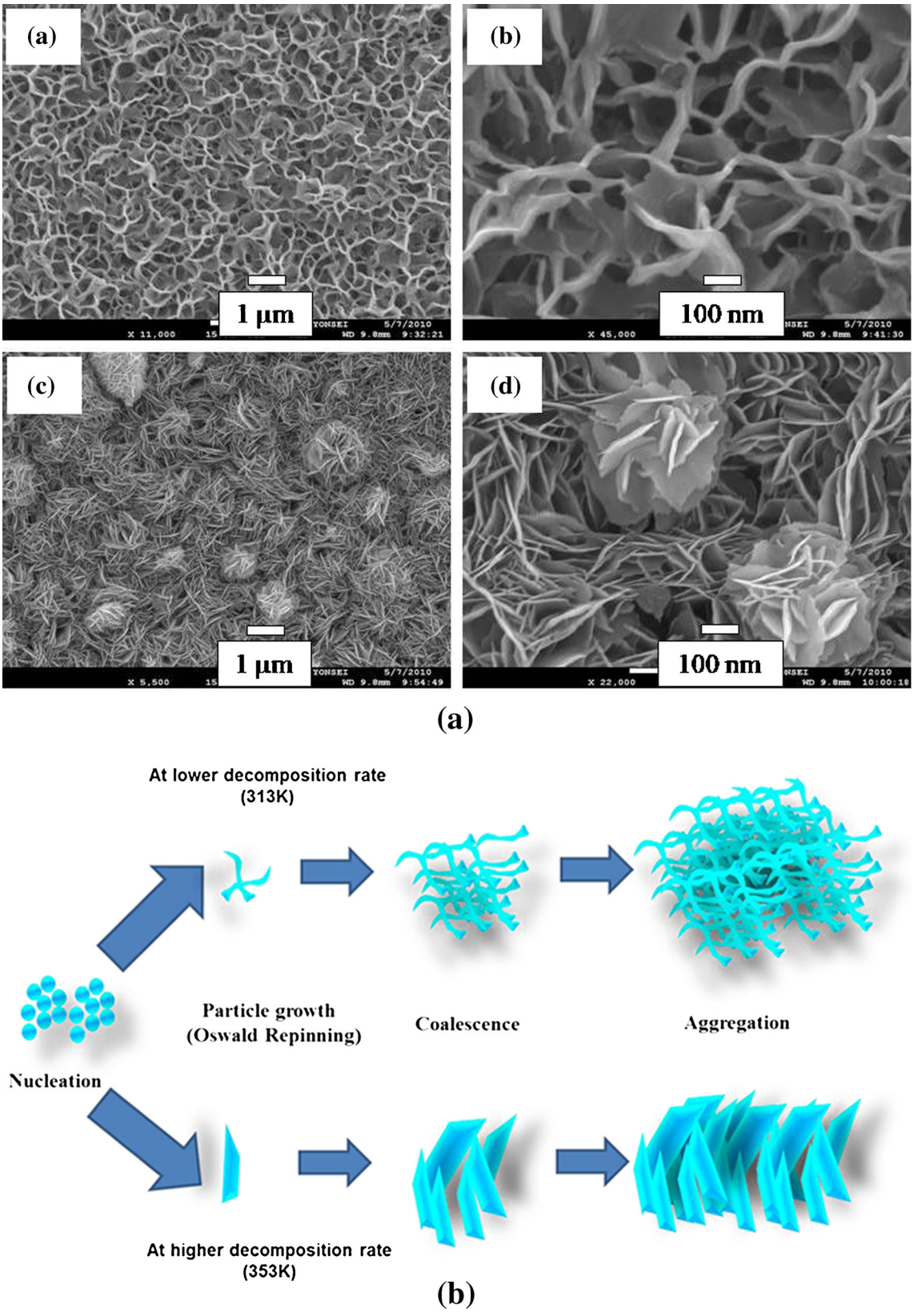

Figure 3. (**a**) SEM images of nickel hydroxide prepared at (a, b) 313 and (c, d) 353 K bath temperatures. (**b**) Schematic diagram of growth model for nickel hydroxide thin films prepared at different bath temperatures.

like microstructure. Pawar *et al* (2010) also reported bath temperature effect onto morphology of ZnO, altered from fibrous flakes into rod-like microstructure.

3.4 *Supercapacitive behaviour of $Ni(OH)_2$ thin film*

The distinctive morphology plays a basic role in supercapacitor, it provides easy accessibility to electrolyte OH^- ions to $Ni(OH)_2$ active material and a fast diffusion rate within the redox phase. It is believed that the unique morphological foundation is one of the key parameters to improve specific capacitance (Yan *et al* 2012). Therefore, CBD deposited different nanostructured $Ni(OH)_2$ electrodes were used in the supercapacitor and their performance were tested using cyclic voltammetry (CV), charge–discharge curve and electrochemical impedance analysis (EIS). The supercapacitive study was carried out by means of effect of scan rate on specific capacitance. The specific capacitance (F/g) of the electrode was obtained by dividing the capacitance to weight dipped in the electrolyte.

Figure 4 shows CV curves of $Ni(OH)_2$ thin films. The redox couple from CV indicates that the capacitance characteristic of electrode is different from that of electric double-layer capacitance, which is normally close to an ideal rectangular shape. This outcome suggests that the capacitance of $Ni(OH)_2$ mainly results from a pseudo-capacitive behaviour. There were two clear redox peaks P1 and P2 in CV curves. The anodic peak P1 was due to the oxidation of $Ni(OH)_2$ to NiOOH and the cathodic peak P2 was for the reverse process. The oxidation and reduction peaks are at different potentials for samples N1 (figure 4(a)) and N2 (figure 4(b)). These differences in reduction and oxidation potentials for both samples are due to thin film containing different phases of $Ni(OH)_2$ material. For (α and β) mixed phase electrode N1, the oxidation peak observed at 0·4 V/SCE and reduction peak at 0·25 V/SCE, such oxidation and reduction processes at lower potentials are attributed to the presence of α phase of $Ni(OH)_2$ in the film (Lang *et al* 2010). However, figure 4(b) shows CV curves of sample N2, it reveals oxidation potential at 0·48 V/SCE and reduction potential at close to 0·35 V/SCE. Similar redox potentials were reported for β-$Ni(OH)_2$ (Patil *et al* 2009), this result confirms that sample N2 contains pure β phase of $Ni(OH)_2$. The appearance of anodic and cathodic peaks corresponding to the $Ni(OH)_2$/NiOOH redox reaction in CV is according to the following electrochemical reaction:

$$Ni(OH)_2 + OH^- \leftrightarrow NiOOH + H_2O + e^-. \quad (4)$$

As an effect of scan rate, shown in figure 4(a), interestingly shifting of oxidation and reduction peaks for N1 sample is observed. Moreover, currents of all scan rates for $Ni(OH)_2$ electrodes increased rapidly at the positive sweep potential range. When the scan rate increased, the anodic peak P1 almost disappeared. Such change in oxidation may be due to the unstable nature of α phase $Ni(OH)_2$ (Chen and Gao 2005). Because, the electrode cannot bear the higher scan rate. At high scan rate, ions on the electrode are depleted rapidly with increasing current, while ions in the electrolyte solution diffuse too slowly to satisfy the need for ions near the interface during the charging and discharging process (Gujar *et al* 2007).

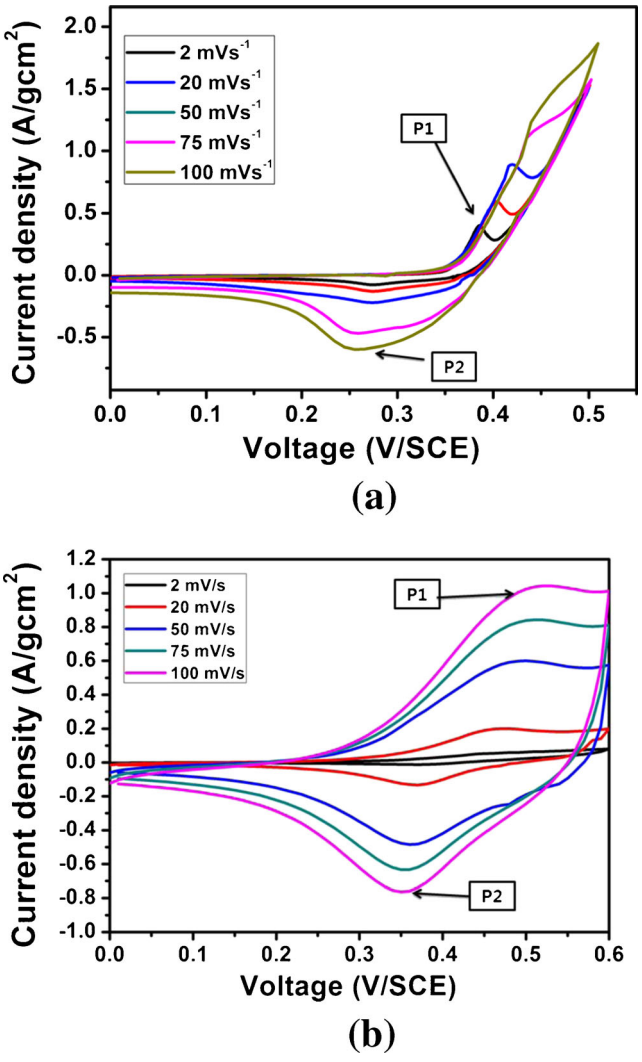

Figure 4. Cyclic voltammograms (CV) of nickel hydroxide electrodes prepared at (**a**) 313 and (**b**) 353 K for different scanning rates in 1 M KOH electrolyte.

Figure 5 shows variation of specific capacitance with respect to scan rate. The graph shows a maximum achieved specific capacitance of about 610 F/g for sample N2 at lowest scan rate, 2 mV/s. Whereas, a maximum specific capacitance of up to 460 F/g at a scan rate 2 mV/s is seen in sample N1. However, sample N1 shows a stable capacitance at higher scan rate as compared to sample N2. It is mainly because of the distinctive surface morphology of sample N1. Generally, at higher scan rate, capacitance decreases drastically because of inner active sites which cannot sustain the redox transitions completely at higher scan rates. This is probably due to the diffusion effect of charges within the electrode. The decreasing capacitance suggests that parts of the surface of the electrode are inaccessible at high charging–discharging

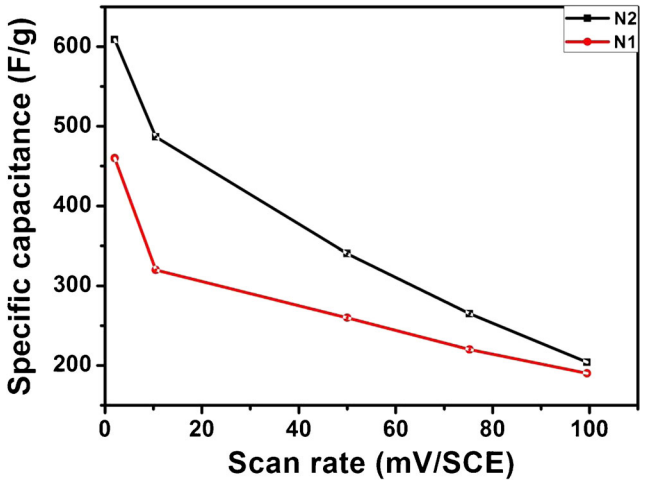

Figure 5. Plots of variation of specific capacitance with scan rate for samples (N1) 313 and (N2) 353 K.

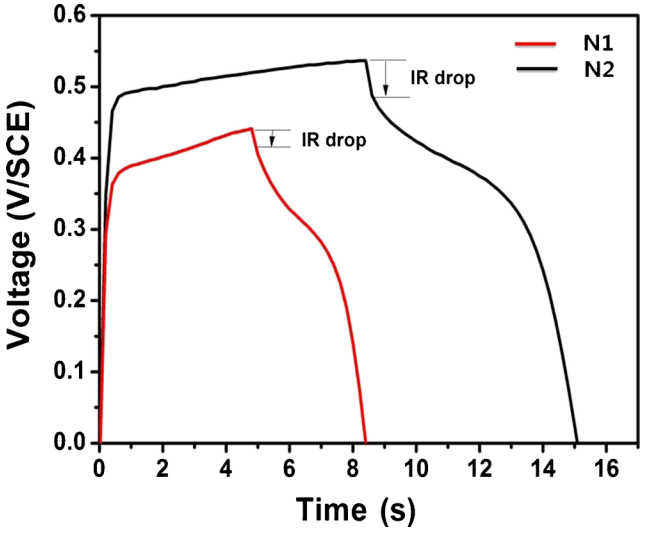

Figure 6. Charge–discharge curves of nickel hydroxide thin films for samples (N1) 313 and (N2) 353 K at 0·5 mA/cm^2.

rates (Gujar *et al* 2007). Honeycomb-like morphology of sample N1 can provide large surface area for easy accessibility of ions from electrolyte; it resulted in good sustainability of electrode at higher scan rate.

Figure 6 shows charge-discharge curves of samples N1 and N2. Charge/discharge galvanostatic plot measured at 0·5 mA/cm^2 is shown in figure 6. The observed nonlinearity in charge–discharge profile, which deviates from the typical linear variation of voltage with time, normally exhibited by EDLCs, can be explained as due to the pseudocapacitance arising out of the redox reaction at this voltage range (Li *et al* 2012). At the beginning of charge and discharge, a sharp change in voltage ($\Delta V1$) is due to the equivalent series resistance (ESR) of the electrochemical capacitor cell. The calculated ESR for N1 and N2 samples are 60 and 160 Ω/cm^2, respectively. Such high ESR calculated from charge–discharge restricts to achieve maximum value of specific capacitance close to theoretical one.

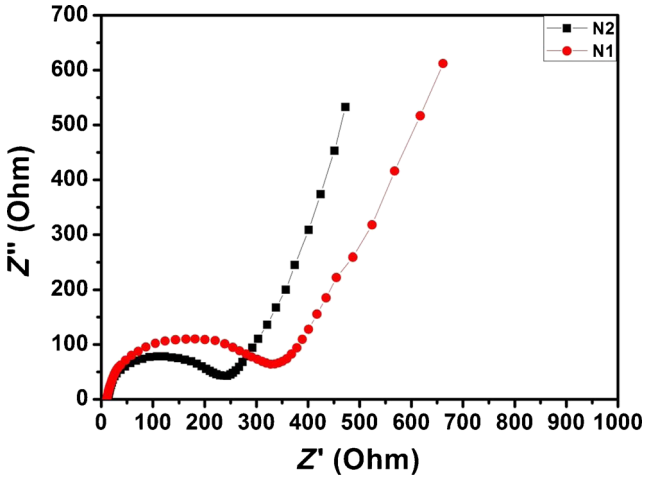

Figure 7. Complex-plane plot of nickel hydroxide electrode in 1 M KOH prepared at (N1) 313 and (N2) 353 K temperatures.

The electrochemical impedance studies (EIS) (in frequency 10^5–10^{-2} Hz) of $Ni(OH)_2$ is carried out in 1 M KOH. The complex-plane plot shown in figure 7 consists of a small semicircle at higher frequencies with a transition to a linear part at low frequencies which corresponds to a capacitive behaviour (Lufrano and Staiti 2010). The electronic resistance is related to the intrinsic electronic resistance of $Ni(OH)_2$ particles and the interfacial resistances of particles-to-particles and particles-to-current collector. An impedance arc of a semicircle is visible in the high frequency region ($\geq$1000 Hz), which can be attributed to the complicated interfaces at $Ni(OH)_2$ particles and $Ni(OH)_2$–substrate contacts, since electron hopping at these interfaces occurs during the charge/discharge processes. At low-frequencies, an approximately vertical increase in Z'' appeared, demonstrating typical capacitive characteristics, which should be governed by the Faradaic reactions of $Ni(OH)_2$ between different oxidation states. From the Nyquist plot one can observe solution resistance (R_s) value is higher for sample N1 as compared with sample N2 ($13 > 9\Omega$) (Adekunle *et al* 2011). The charge transfer resistance (R_{ct}) is also smaller for sample N2 than the sample N1 ($125 < 180\ \Omega$), these results obtained may be due to small electrochemical distribution resistance (EDR) exerted by macroporus structure of honeycomb like morphology (Yang *et al* 2012). Small R_s and EDR values of sample N2 than N1 are imperative for high supercapacitance of sample N2. This result predicts that the charges can easily transfer towards electrode through the vertically grown microflakes instead of honeycomb structure. The results obtained from EIS study gives detailed information of maximum specific capacitance for sample N2 than N1.

4. Conclusions

In summary, different nanostructured $Ni(OH)_2$ thin films were prepared by using chemical bath deposition (CBD)

method at different bath temperatures. It is concluded that the bath temperature strongly influence the structural and morphological properties of $Ni(OH)_2$ thin films. The mixed phases of α and β were prepared at lower bath temperature (N1), however, pure β phase of $Ni(OH)_2$ (N2) were prepared at higher bath temperature. The films deposited at low temperature (N1) showed interconnected honeycomb structure while films deposited at higher temperature (N2) shows well-developed flake-like morphology. Crystal structure and morphology influences on electrochemical performance of the electrode. EIS studies showed that, vertical flake-like morphology is good in supercapacitor application in terms of small charge transfer resistance (R_{ct}) than honeycomb-like morphology. Vertical nanoflakes and its porous structure can provide easy charge transportation through material with stress-free accommodation for ions from electrolyte. Vertically aligned flakes with porous structure showed maximum specific capacitance of 610 F/g.

References

Adekunle A S, Ozoemena K I, Mamba B B, Agboola B O and Oluwatobi O S 2011 *Int. J. Electrochem. Sci.* **6** 4760

Bernard M C, Bernard P, Keddam M, Senyarich S and Takenouti H 1996 *Electrochim. Acta* **41** 91

Cai F S, Zhang G Y, Chen J, Gou X L, Liu H K and Dou S X 2004 *Angew. Chem.* **116** 4308

Cao M, He X, Chen J and Hu C 2007 *Cryst. Growth Des.* **7** 170

Chen D L and Gao L 2005 *Chem. Phys. Lett.* **405** 159

Coudun C and Hochepied J F 2005 *J. Phys. Chem.* **B109** 6069

Gujar T P, Shinde V R, Lokhande C D, Kim W Y, Jung K D and Joo O-S 2007 *Electrochem. Commun.* **9** 504

Gurav K V, Fulari V J, Patil U M, Lokhande C D and Joo O-S 2010 *Appl. Surf. Sci.* **256** 2680

Hodes G 2002 *Chemical solution deposition of semiconductor films* (New York: Marcel Dekker Inc)

Kandalkar S, Dhawale D, Kim C and Lokhande C 2010 *Synth. Met.* **160** 1299

Lang J W, Kong L B, Liu M, Luo Y C and Kang L 2010 *J. Solid State Electrochem.* **14** 1533

Largeot C, Portet C, Chmiola J, Taberna P, Gogotsi Y and Simon P 2008 *J. Am. Chem. Soc.* **130** 2730

Li J, Yang M, Wei J and Zhou Z 2012 *Nanoscale* **4**, 4498.

Liang Z H, Zhu Y J and Hu X L 2004 *J. Phys. Chem.* **B108** 3488

Liu X H, Qiu G Z, Wang Z and Li X G 2005 *Nanotechnology* **16** 1400

Lokhande C D, Park B O, Park H S, Jung K D and Joo O-S 2005 *Ultramicroscopy* **105** 267

Lufrano F and Staiti P 2010 *Int. J. Electrochem. Sci.* **5** 903

Mane R S and Lokhande C D 2000 *Mater. Chem. Phys.* **65** 1

Matsui K, Kyotani T and Tomita A 2002 *Adv. Mater.* **14** 1216

Ni X M, Zhao Q B, Cheng J, Zheng H G, Li B B and Zhang D G 2005 *Chem. Lett.* **34** 1408

Patake V D and Lokhande C D 2008 *Appl. Surf. Sci.* **254** 2820

Patil U M, Gurav K V, Fulari V J, Lokhande C D and Joo O-S 2009 *J. Power Sources* **188** 338

Pawar S M, Gurav K V, Shin S W, Choi D S, Kim I K, Lokhande C D, Rhee J I and Kim J H 2010 *J. Nanosci. Nanotechnol.* **10** 1

Pawar S M, Pawar B S, Kim J H, Joo O-S and Lokhande C D 2011 *Curr. Appl. Phys.* **11** 117

Salunkhe R R, Patil U M, Gujar T P and Lokhande C D 2009 *Appl. Surf. Sci.* **255** 3923

Shinde V R, Gujar T P, Lokhande C D, Mane R S and Han S H 2007 *Mater. Sci. Eng.* **B137** 119

Tong G X, Liu F T, Wu W H, Shen J P, Hu X and Liang Y 2012 *Cryst. Eng. Commun.* **14** 5963

Wang Y, Zhu Q S and Zhang H G 2005 *Chem. Commun.* 5231

Wang G, Zhang L and Zhang J 2012 *Chem. Soc. Rev.* **41** 797

Wu Z C, Zhu X, Pan C, Yao Z Y and Xie Y 2006 *Chinese J. Inorg. Chem.* **22** 1371

Yan J *et al* 2012 *Adv. Funct. Mater.* **22** 2632

Yang D, Wang R, Zhang J and Liu Z 2004 *J. Phys. Chem.* **B108** 7531

Yang L X, Zhu Y J, Tong H, Liang Z H and Wang W 2007 *Cryst. Growth Des.* **7** 2716

Yang S, Wu X, Chen C, Dong H, Hu W and Wang X 2012 *Chem. Commun.* **48** 2773